Article:
Cheshire, D., Bencok, P., Gianolio, D. et al. (4 more authors) (2022) Absence of spin-mixed states in ferrimagnet Yttrium iron garnet. Journal of Applied Physics. 103902. ISSN: 1089-7550

https://doi.org/10.1063/5.0099477

Journal of Applied Physics

Absence of spin-mixed states in ferrimagnet Yttrium iron garnet

Cite as: J. Appl. Phys. **132**, 103902 (2022); https://doi.org/10.1063/5.0099477
Submitted: 24 June 2022 • Accepted: 11 August 2022 • Published Online: 14 September 2022

D. Cheshire, P. Bencok, D. Gianolio, et al.

AIP Publishing

Journal of Applied Physics ARTICLE scitation.org/journal/jap

Absence of spin-mixed states in ferrimagnet Yttrium iron garnet

Cite as: J. Appl. Phys. **132**, 103902 (2022); doi: 10.1063/5.0099477
Submitted: 24 June 2022 · Accepted: 11 August 2022 ·
Published Online: 14 September 2022

D. Cheshire,[1] P. Bencok,[2] D. Gianolio,[2] G. Cibin,[2] V. K. Lazarov,[1] G. van der Laan,[2] and S. A. Cavill[1,a)]

AFFILIATIONS

[1]Department of Physics, University or York, Heslington, York YO10 5DD, United Kingdom
[2]Diamond Light Source, Harwell Science and Innovation Campus, Chilton, Didcot OX11 ODE, United Kingdom

[a)]**Author to whom correspondence should be addressed:** stuart.cavill@york.ac.uk

ABSTRACT

The spectroscopic g-factor of epitaxial thin film Yttrium Iron Garnet (YIG) has been studied using a combination of ferromagnetic resonance spectroscopy and x-ray magnetic circular dichroism. The values obtained by the two techniques are found, within experimental error, to be in agreement using Kittel's original derivation for the g-factor. For an insulating material with an entirely Fe^{3+} configuration, a spin mixing correction to Kittel's derivation of the spectroscopic g-factor, as recently shown by Shaw *et al.* [Phys. Rev. Lett. **127**, 207201 (2021)] for metallic systems, is not required and demonstrates that the spin mixing parameter is small in YIG due to negligible spin–orbit coupling.

I. INTRODUCTION

The efficient generation and control of spin currents are key drivers in spintronics research. Current focus has been directed at spin–orbit coupling (SOC) to achieve both[1] and has led to a rapid rise in the sub-field of spin-orbitronics. SOC manifests itself in many observables of fundamental importance and is responsible for a variety of phenomena in ferromagnets and heavy metals such as magnetocrystalline anisotropy, the spin Hall effect, and the spin mixing of electronic states.[2–6] Regarding the latter, the spin mixing parameter, b^2, is central to the Elliot–Yafet theory of spin relaxation where the spin-relaxation time T_1 is related to the Drude relaxation time τ via b^2 such that $T_1 = \frac{\tau}{pb^2}$[7] and p is a proportionality constant in the order one. The SOC-induced spin mixing has also been shown to determine the damping of ultrafast magnetization dynamics.[8] However, in order to obtain the values of the spin–orbit coupling constant, it is necessary to quantify or at least obtain a ratio of the spin and orbital moments in a magnetic material. This is particularly important in thin films where interfaces and reduced symmetries can have dramatic effects.[9] Ferromagnetic resonance (FMR) spectroscopy and x-ray magnetic circular dichroism (XMCD) are the two primary techniques used to determine the ratio of orbital and spin moments. Assuming the spin moment (μ_S) is known *a priori*, the orbital moment (μ_L) can be obtained via the FMR spectroscopic g factor using[10]

$$\frac{\mu_L}{\mu_S} = \frac{g-2}{2}. \quad (1)$$

By employing synchrotron-based core level spectroscopy such as XMCD, the orbital and spin moments can also be obtained via the magneto-optical sum rules,[11] allowing for a complementary measurement of both the orbital to spin moment ratio and the spectroscopic g factor. However, recent work by Shaw *et al.*[12] has highlighted that the orbital to spin moment ratio, determined by the two techniques, differs for ferromagnetic metals. In order to reconcile the differences, the authors suggest and provide evidence that a modification of Kittel's equation [Eq. (1)], relating g to the ratio of the orbital and spin moments, is required. This modification, an additional higher order term to Eq. (1), takes into account the spin mixing of states, which Kittel originally ignored as a weak second-order effect. Motivated by the findings,[12] in this Letter, we report and compare values of g obtained using both XMCD and in-plane VNA-FMR spectroscopy for a single crystalline YIG thin film. Ratios of orbital-to-spin moment (and g) found with both methods are shown to agree within experimental error using Kittel's original equation. It is shown that higher-order corrections involving b^2—used to account for spin-mixing in ferromagnets

such as Co and Ni[12]—are very small (if not zero) for the insulating ferrimagnet YIG that contains Fe^{3+}.

II. SAMPLE FABRICATION

The crystalline YIG film was grown by pulsed laser deposition (PLD) on a (111)-oriented gadolinium gallium garnet (GGG) substrate. An amorphous YIG layer was deposited at room-temperature in a chamber with a partial oxygen pressure of 2.5×10^{-3} mbar, ablating a stoichiometric polycrystalline YIG target. The frequency quadrupled Nd:YAG ablation laser operated at a wavelength of 266 nm with a repetition frequency of 10 Hz and fluence of approximately 3.0 J cm^{-3} (100 mJ per pulse). The sample was steadily rotated during deposition at 6 RPM. Post-deposition, the amorphous YIG/GGG sample was annealed *ex situ* in a tube furnace. Following Ref. 13, annealing was performed in air (atmosphere) at 650 °C for 3 h, after which a crystalline YIG thin film was produced. An additional 2 nm platinum capping layer was deposited after FMR measurements were performed to allow total electron yield (TEY) detection for XAS/XMCD spectroscopy. We note that the addition of Pt did not affect the value of the g factor obtained by FMR. The Pt layer was grown at room-temperature using PLD, by ablating a pure Pt target in vacuum at a base pressure of 8×10^{-8} mbar.

III. EXPERIMENTAL RESULTS

A. XRD

The YIG thin film was structurally characterized using x-ray diffraction (XRD) around the (444) reflection to confirm epitaxial crystallization of the YIG on the GGG substrate. As bulk materials, the lattice mismatch between YIG and GGG is minimal ($\Delta a = 0.06\%$). As shown in Fig. 1, the corresponding overlap expected between YIG and GGG Bragg reflections is evidenced by the presence of Pendellösung oscillations close to GGG (444) reflection. The overlap is so significant that the YIG and GGG peaks cannot be individually separated. Transmission electron microscopy (TEM) cross-sectional images at the YIG/GGG interface, see inset of Fig. 1, indicate high-quality epitaxial growth of YIG on GGG. The interface is seen to be smooth, with interfacial roughness below 1 nm and minimal lattice mismatch between the YIG and GGG. X-ray reflectivity (XRR) measurements were performed to determine the thickness and average roughness for the YIG layer. Measurements were performed by scanning $2\theta - \omega$ below 6°, and the acquired reflectivity fringes were fitted using the GenX software package.[14] XRR of the YIG layer was measured prior to the deposition of Pt to avoid the higher density Pt dominating the XRR response. Measured and fitted Kiessig fringes are shown in Fig. 2, with an accompanying scattering length density (SLD) simulation from the extracted fitting parameters. For the fitting procedure, fixed densities of 7.08 and 5.17 g cm^{-3} were used for GGG and YIG, respectively. From Fig. 2, an average YIG thickness of (49.9 ± 0.1) nm was obtained with an RMS roughness of (0.6 ± 0.1) nm. GGG substrate roughness came to a similar value at (0.7 ± 0.1) nm, in agreement with the TEM image in Fig. 1.

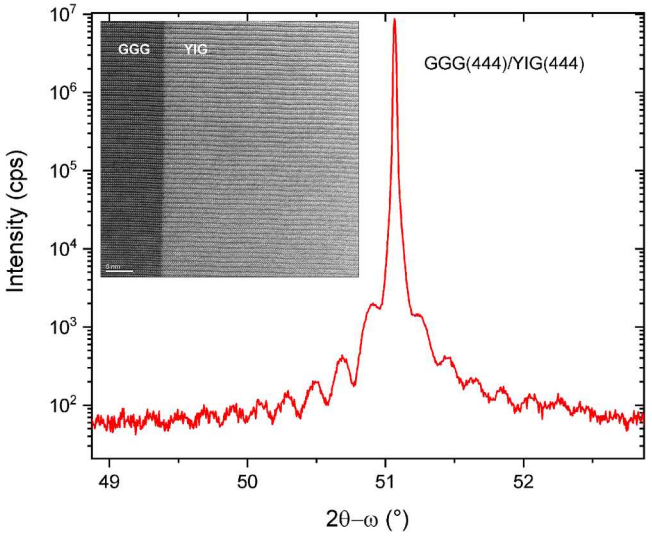

FIG. 1. 2θ – ω XRD measurement about the (444) reflection for YIG(50 nm)/GGG(111). Inset: Cross-sectional TEM images of the YIG/GGG interface, along the [11–2] zone axis.

B. FMR

The spectroscopic g-factor was obtained using vector network analyzer (VNA)-based FMR spectroscopy for an in-plane geometry. Placing the YIG sample face down on the co-planar waveguide, the microwave transmission parameter, S_{12}, was measured over a frequency range of 0.001–15 GHz in 1601 equally spaced frequency

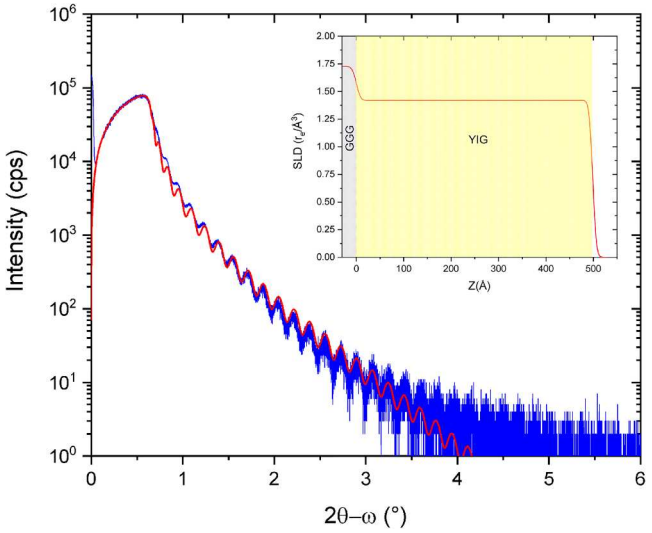

FIG. 2. XRR measurement (blue) with a fitted curve (red) for YIG/GGG. Inset shows SLD against sample depth (Z) simulated from the XRR fitting parameters for YIG/GGG.

steps. A magnetic field range of 0–3 kOe was covered with a field step of 0.1 Oe to measure resonance below 15 GHz. All VNA-FMR measurements were performed at an RF power of +7 dBm. Linescans at constant frequency were extracted from the FMR frequency-field maps and fitted using an asymmetric Lorentzian function[15] to determine the corresponding resonance field (H_r). The resonance frequency as a function of field is fit to the easy-axis in-plane Kittel equation for a (111) orientated film, given by

$$\omega = 2\pi\gamma\sqrt{H(H + 4\pi M_{eff})}, \tag{2}$$

where the gyromagnetic ratio, $\gamma = g\mu_B/\hbar$, and M_{eff} is the effective magnetization where $4\pi M_{eff} = 4\pi M_S - \frac{K}{M_s}$, M_s is the saturation magnetization (136 ± 1 emu/cc), and K is the cubic magnetocrystalline anisotropy constant (−6100 erg/cc for YIG).[16] M_s determined from the Kittel curve fit agrees within error with independent magnetometry measurements of the sample using vibrating sample magnetometry.[17]

An exemplar frequency-field map recorded along the [11$\bar{2}$] easy axis is shown in Fig. 3, with a 10 GHz linescan inset. A narrow resonance of ΔH(10 GHz) = (6.0 ± 0.2) Oe was measured at an H_r of 2740 ± 1 Oe. Following Refs. 18 and 19, the gyromagnetic ratio γ is determined by fitting the Kittel curve with Eq. (2) yielding γ = (2.83 ± 0.02) MHz/Oe and M_{eff} of (140 ± 1) emu/cc in agreement with other YIG FMR studies.[13] γ is close to the free-electron value of 2.802 MHz/Oe and agrees well with other FMR studies of YIG deposited by various techniques: PLD,[20] sputtering,[21] and LPE.[22] From the gyromagnetic ratio, a g-factor of 2.02 ± 0.01 is obtained. This g-factor is consistent with Ref. 22, where an anisotropic g-factor is measured to be of 2.022 from in-plane FMR and 2.012 from out-of-plane FMR (averaged to a g of 2.016). Similar g-factors are reported in Ref. 20.

C. XAS and XMCD

XAS and XMCD spectroscopy was performed on the BLADE (I10) beamline at the Diamond Light Source. The XAS/XMCD was measured at Fe $L_{2,3}$ absorption edges in order to determine valency, co-ordination, and the magnetic properties of Fe cations. In L-edge XAS, electrons are excited from a 2p core level to the unoccupied 3d valence states of the element of interest by circular polarized x rays at the resonant transition energies. The difference in absorption for opposite circular polarizations (XMCD) gives a direct and element-specific measurement of the projection of the 3d magnetic moment along the x-ray polarization vector.[11] The absorption cross section is conventionally obtained by measuring the decay products, typically electrons in TEY, of the photo-excited core hole. The type of decay product measured determines the probing depth of the technique, and for transition metals at $L_{2,3}$ absorption edges, the probing depth in TEY detection is approximately 3–6 nm. All measurements were performed at normal incidence, in order to reduce the effect of self-absorption on the spectra,[23] and in a 5 T field applied collinear to the photon helicity vector. XAS and XMCD spectra are shown in Fig. 4. The XMCD line shape agrees well with other YIG XMCD found in the literature.[24,25] Integration of the XMCD and application of the XMCD sum rules,

$$\frac{\mu_L}{\mu_S} = \frac{2q}{9p - 6q}, \tag{3}$$

where p and q are the integrated intensities of the XMCD over

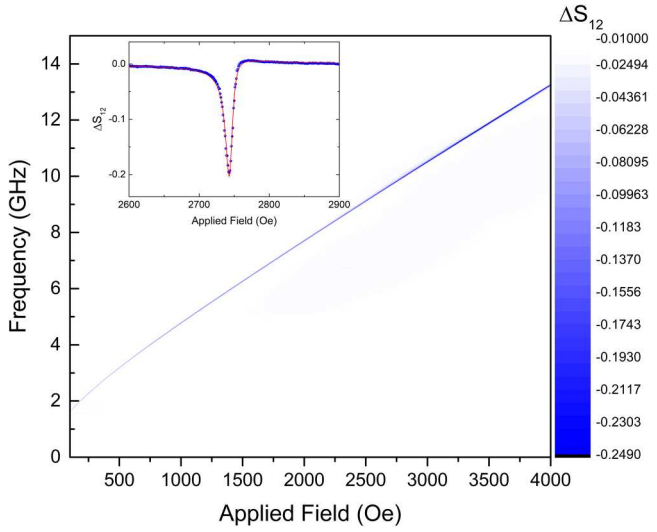

FIG. 3. In-plane VNA-FMR frequency-field map for the YIG/GGG thin film. Inset shows a field linescan taken at 10 GHz and fitted to an asymmetric Lorentzian function.

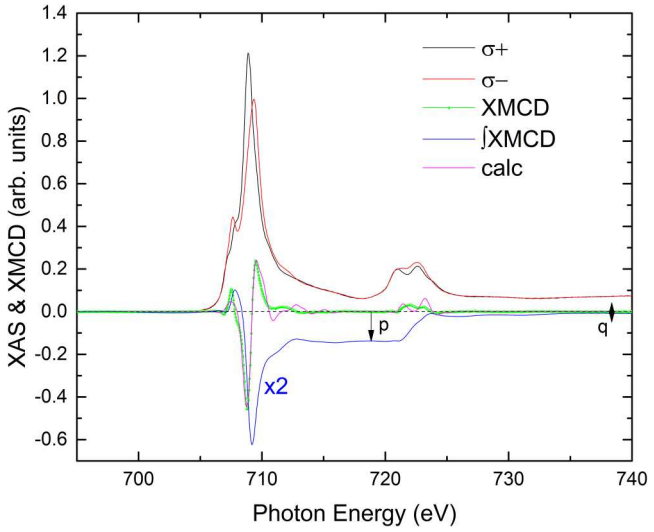

FIG. 4. Experimental XAS/XMCD spectra with XMCD integral for a 50 nm YIG/GGG thin film. TEY at normal incidence in H = 5 T at 300 K. A calculated fit to the Fe $L_{3,2}$ XMCD from atomic multiplet calculations is also shown.

$L_3$and $L_{2,3}$ edges, respectively, yield values of $(\mu_L/\mu_S) = 0.012 \pm 0.006$.[26] The value of q in the XMCD integral is proportional to the orbital magnetic moment contribution, which is almost completely quenched in the YIG film. This follows the expected zero orbital moment for a $3d^5$ configuration. The small deviation from zero may arise from hybridization of Fe cations with the ligands. A corresponding g-factor of 2.02 ± 0.01 is calculated from the XMCD ratio of orbital-to-spin moment using Eq. (1), which is consistent with our FMR data and (Ref. 25) where a g-factor of 2.01 was obtained via a similar XMCD sum rules analysis of YIG. We note that the Pt capping layer may introduce an orbital moment that is measured by the surface-sensitive XMCD but not the bulk-sensitive FMR. However, given the spectroscopic g-factors agree within error, we conclude that an induced orbital moment, if any, is very small and well within the uncertainty of our measurement. A further indication of this conclusion stems from the fact that the XMCD spectra measured in this study are identical to that measured in Ref. 25, where there was no capping layer.

Contributions to YIG magnetism from tetrahedral and octahedral Fe^{3+} sites were evaluated from atomic multiplet calculations using the CTM4XAS software.[27] Following Ref. 28, a Slater parameter reduction of 70%, 80%, and 80% was used, with a 10Dq value of 1.6 and −0.6 eV for O_h and T_d co-ordination, respectively. A Lorentzian broadening of 0.15 eV was used for the L_3 edge and 0.3 eV for the L_2 edge, with Gaussian broadening of approximately 0.2 eV. As shown in Fig. 4, the atomic multiplet calculations have a high level of agreement with the experimental XMCD data at the L_3 edge for a relative occupation of 0:60:40 (Fe^{2+} O_h:Fe^{3+} T_d:Fe^{3} O_h), with a 5% tolerance on each. This is the expected 3:2 ratio of T_d:O_h Fe^{3+} in stoichiometric YIG. The Fe^{2+} contribution is zero. It is worth noting that the small disagreement between the theory and experiment for the spectral structure is mainly due to effects that are not included in the calculation. The linewidth broadening of each individual peak depends on its decay probability. This increases gradually with higher photon energies as for the excited state increasingly more decay channels open up. Also, the calculation does not include hybridization with configurations that are higher in energy and their presence might, therefore, be responsible for spectral differences in the range of 710–715 eV. The spectral appearance of the L_2 edge can be changed by the Coster–Kronig interaction between the discrete states $2p_{1/2}3d^n$ and continuum states $2p_{3/2}3d^{n-1}k$, where k is a continuum electron. This interaction has not been accounted for in the calculated spectra except for a larger Lorentzian line broadening for the L_2 structure; however, it should also influence the spectral shape. As a result, although the calculation is reliable for the peaks of interest in the L_3 region, the structure at higher energies is less suitable for the quantitative analysis.

Additional hard x-ray absorption was performed on the core XAS beamline B18 at the Diamond Light Source. XANES was measured over the Fe K-edge to probe the bulk of the film and provide complementary information on the valence of Fe cations in the YIG film. The sample was mounted at approximately 45° to the incident x-ray beam (beam size, $200 \times 250\,\mu m^2$), and x-ray fluorescence was measured as the incident x-ray energy was swept from 6.8 to 7.5 keV. Fluorescence data were collected in the continuous scan mode using an emission spectrometer in dispersive Von Hamos geometry and a Medipix quad chip detector. The spectrometer was configured to focus the Fe K_α signal (while photons of different energies were defocused) and a region of interest was defined around the focal point to extract the fluorescence counts from the images acquired for each energy point. The use of the spectrometer offered a better energy resolution with respect to a monolithic Ge detector and helped remove the interference from substrate diffraction peaks in the XAS spectrum. 16 separate scans were averaged to improve the signal-to-noise ratio. XAS data over the Fe K-edge are shown in Fig. 5. The dominant Fe valence was inferred from the analysis of the 1s to 3d pre-edge XANES feature, following the methods of Refs. 29 and 30. XAS data were normalized using the ATHENA program[31] at the K-edge step. A spline fit to the tail of the absorption edge was subtracted as a background to isolate the 1s to 3d pre-edge feature. The spectral shape of the pre-edge feature was fitted to a convolution of two pseudo-Voigt functions to evaluate Fe^{2+} and Fe^{3+} species contributions: initially centered at 7112 and 7114.5 eV, respectively, with Gaussian and Lorentzian contributions allowed to vary. All fittings tended toward a single Gaussian of Fe^{3+} valence with an energy centroid of 7114.2 eV. The lack of convolution in the pre-edge spectral shape (and fit) indicates a very high $Fe^{3+}/\Sigma Fe$ ratio approaching 1; an $Fe^{3+}/\Sigma Fe$ of 0.87 still shows significant skew from 7114 eV toward lower x-ray energies,[29] which is not evident in the data presented here. An $Fe^{3+}/\Sigma Fe$ approaching 1 also agrees with atomic multiplet calculations fitted to the XMCD data, where Fe^{2+} contributions are zero.

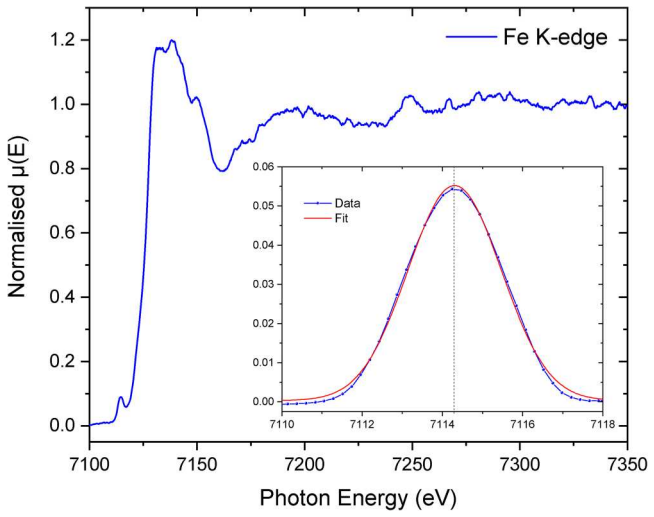

FIG. 5. XAS for YIG/GGG taken over the Fe K-edge. Inset shows pre-edge XANES 1s → 3d transition feature, following spline subtraction. Peak fitting tends to a Gaussian centered at 7114.2 eV, indicating a $Fe^{3+}/\Sigma Fe$ approaching 1.

IV. DISCUSSION

As discussed earlier, the recent work on Co and Ni thin films has demonstrated large discrepancies between the g factor obtained from FMR and XMCD measurements,[12] with a second-order spin

mixing correction to the original derivation of g[10] required to reconcile the two experimental values. Although such discrepancies were found to be smaller in metallic Fe thin films, they are still considered large enough that second-order corrections are deemed necessary. Blume *et al.*[32] had also shown that second-order corrections are needed when considering electron paramagnetic resonance (EPR) of some transition metal ions in paramagnetic salts. According to Ref. 30, the spectroscopic splitting factor g may be written as

$$g = (L_z + 2S_z)/S'_z, \tag{4}$$

where S'_z is the z component of the fictitious spin in the spin Hamiltonian and S_z is the expectation value of the real spin. To first order in the SOC coupling, i.e., to $(0|\boldsymbol{H}\cdot\boldsymbol{L}|n)(n|\lambda\boldsymbol{L}\cdot\boldsymbol{S}|0)/\Delta$, where $|0\rangle$ is the ground state, $|n\rangle$ is the excited state, and Δ is the energy difference between ground and excited states, $S'_z = S_z$, which re-produces Eq. (1). However, to second order in λ (i.e., for non-zero b^2 terms), the initial spin state $|S_z\rangle$ may be mixed with $|S_z+1\rangle$ and $|S_z-1\rangle$ so that $S'_z \neq S_z$ requiring b^2 corrections to Eq. (1), which can be sensitive to the crystal field. Co^{2+} in octahedral crystal fields is an example in which $S'_z \neq S_z$, and Eq. (1) requires corrective second-order terms.[10,32]

Using Eq. (1), our data show that FMR and XMCD yield the same value of the spectroscopic g factor for Fe^{3+} in YIG within the associated experimental error of each technique. For an insulating material with an entire Fe^{3+} configuration, a spin mixing correction following Ref. 12 is not required for the g-factor obtained by XMCD. To first order, the orbital moment should be zero for $3d^5$ configuration leading to negligible first-order SOC.[10,32] The spin mixing of states is a second-order effect and arises from the second term on the right hand side of the spin–orbit operator as shown in Eq. (5),

$$\lambda\boldsymbol{L}\cdot\boldsymbol{S} = \lambda\left[L_zS_z + \frac{1}{2}(A_LB_s + B_LA_s)\right], \tag{5}$$

where A and B are the raising and lowering operators that mix the upper states with the ground state. The small value of λ for Fe^{3+} (0.05 eV) and large energy separation, ≈3 eV, between the $^6S_{5/2}$ ground state and the $^4P_{5/2}$ excited state (which is the obvious mixing state due to the same J) provides the reason for negligible spin mixing; the spin–orbit coupling constant is small and the energy-level separation between ground and excited states is large. As such, one would intuitively expect a spectroscopic g factor close to the free electron value of 2 and observed in both the experimental FMR and XMCD measurements without the need of second-order corrections, in agreement with the experimental data. However, we note that the experimental uncertainties also translate into an uncertainty in b^2. For completeness, we include the spin mixing of states into Kittel's original equation so that Eq. (1) may now be written as[12]

$$g \approx 2\left(1 + \frac{\mu_L}{\mu_S}\right) - 4[b^2]. \tag{6}$$

Figure 6 shows the effect of the spin mixing parameter, b^2, on the spectroscopic g-factor. From the overlap of error bounds, we obtain a lower and upper limit for b^2 as 0 and 0.006, respectively. Even the upper limit is significantly lower than the value of the spin mixing parameter obtained for ferromagnetic metals[12] (0.02 for CoFe and Py).

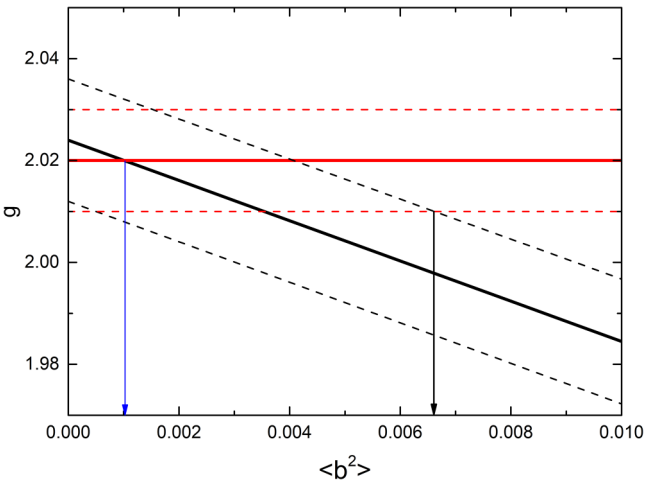

FIG. 6. (Black) Spectroscopic g-factor as a function of the spin mixing parameter obtained from Eq. (6) and the XMCD data. (Red) Spectroscopic g-factor obtained from the FMR data. Error bounds are shown as dashed lines.

Further work in order to verify the validity of Eq. (1) for other ferromagnetic oxides, both conducting and insulating/semiconducting, will enable the importance of spin mixing corrections to the spectroscopic g factor, measured by XMCD, to be obtained across a wide range of materials via simple ionic substitutions.

ACKNOWLEDGMENTS

The authors acknowledge Diamond Light Source for beamtime on beamline I10 under MM22550 and beamline B18 under SP24930.

AUTHOR DECLARATIONS

Conflict of Interest

The authors have no conflicts to disclose.

Author Contributions

D. Cheshire: Formal analysis (equal); Writing – original draft (equal); Writing – review & editing (supporting). **P. Bencok:** Investigation (equal); Writing – original draft (supporting). **D. Gianolio:** Investigation (equal); Writing – original draft (supporting). **G. Cibin:** Investigation (supporting). **V. K. Lazarov:** Investigation (supporting). **G. van der Laan:** Investigation (equal); Writing – original draft (equal). **S. A. Cavill:** Conceptualization (lead); Formal analysis (lead); Investigation (equal); Supervision (lead); Writing – original draft (equal); Writing – review & editing (lead).

DATA AVAILABILITY

The data that support the findings of this study are available from the corresponding author upon reasonable request.

REFERENCES

[1]S. A. Cavill *et al.*, Phys. Rev. Lett **124**, 236803 (2020).
[2]J. C. Slonczewski, Phys. Rev. **101**, 1341 (1958).
[3]J. E. Hirsch, Phys. Rev. Lett. **83**, 1843 (1999).
[4]J. Sinova *et al.*, Rev. Mod. Phys. **87**, 1213 (2015).
[5]J. Fabian and S. Das Sarma, Phys. Rev. Lett. **81**, 5624 (1998).
[6]B. Zimmermann *et al.*, Phys. Rev. B. **93**, 144403 (2016).
[7]R. J. Elliott, Phys. Rev. **96**, 266 (1954).
[8]D. Steiauf and M. Fahnle, Phys. Rev. B **79**, 140401 (R) (2009).
[9]F. Hellman *et al.*, Rev. Mod. Phys. **89**, 025006 (2017).
[10]C. Kittel, Phys. Rev. **6**, 743 (1949).
[11]B. T. Thole *et al.*, Phys. Rev. Lett. **68**, 1943 (1992);P. Carra *et al.*, Phys. Rev. Lett. **70**, 694 (1993);C. T. Chen, *et al.*, Phys. Rev. Lett. **75**, 152 (1995);G. van der Laan and A. I. Figueroa, Coord. Chem. Rev. **277-278**, 95 (2014).
[12]J. M. Shaw, R. Knut, A. Armstrong, S. Bhandary, Y. Kvashnin, D. Thonig, E. K. Delczeg-Czirjak, O. Karis, T. J. Silva, E. Weschke, H. T. Nembach, O. Eriksson, and D. A. Arena, Phys. Rev. Lett. **127**, 207201 (2021).
[13]C. Hauser, T. Richter, N. Homonnay, C. Eisenschmidt, M. Qaid, H. Deniz, D. Hesse, M. Sawicki, S. G. Ebbinghaus, and G. Schmidt, Sci. Rep. **6**, 20827 (2016).
[14]M. Bjork and G. Andersson, J. Appl. Crystallogr. **40**, 1174 (2007).
[15]C. J. Love *et al.*, Appl. Phys. Lett. **119**, 172404 (2021).
[16]P. Hansen, J. Appl. Phys. **45**, 3638 (1974).
[17]M_s, determined by vibrating sample magnetometry, is (130 ± 5) emu/cc, which is within the error of the value determined by FMR with a cubic anisotropy constant K = −6100 erg/cc.
[18]H. Chang, P. Li, W. Zhang, T. Liu, A. Hoffmann, L. Deng, and M. Wu, IEEE Magn. Lett. **5**, 6882836 (2014).
[19]T. Liu, H. Chang, V. Vlaminck, Y. Sun, M. Kabatek, A. Hoffmann, L. Deng, and M. Wu, J. Appl. Phys. **115**, 17A501 (2014).
[20]B. Heinrich, C. Burrowes, E. Montoya, B. Kardasz, E. Girt, Y. Song, Y. Sun, and M. Wu, Phys. Rev. Lett. **107**, 066604 (2011).
[21]C. Dubs, O. Surzhenko, R. Linke, A. Danilewsky, U. Brückner, and J. Dellith, J. Phys. D: Appl. Phys. **50**, 204005 (2017).
[22]S. A. Manuilov, S. I. Khartsev, and A. M. Grishin, J. Appl. Phys. **106**, 123917 (2009).
[23]R. Nakajima, J. Stohr, and Y. U. Idzerda, Phys. Rev. B. **59**, 6421 (1999).
[24]B. B. Krichevtsov, S. V. Gastev, S. M. Suturin, V. V. Fedorov, A. M. Korovin, V. E. Bursian, A. G. Banshchikov, M. P. Volkov, M. Tabuchi, and N. S. Sokolov, Sci. Technol. Adv. Mater. **18**, 351 (2017).
[25]H. B. Vasili, B. Casals, R. Cichelero, F. Macià, J. Geshev, P. Gargiani, M. Valvidares, J. Herrero-Martin, E. Pellegrin, J. Fontcuberta, and G. Herranz, Phys. Rev. B **96**, 014433 (2017).
[26]XMCD sum rules actually provides $\mu_{Seff} = \mu_S + 7\langle T_z \rangle$, where $\langle T_z \rangle$ is the expectation value of the magnetic dipole operator. In bulk cubic ferromagnets, $\langle Tz \rangle$ is vanishingly small and we ignore this term in our analysis due to the relatively thick YIG layer (40 nm).
[27]E. Stavitski and F. M. F. de Groot, Micron **41**, 687 (2010).
[28]P. Kuiper, B. G. Searle, L. C. Duda, R. M. Wolf, and P. J. Van Der Zaag, J. Electron Spectros. Relat. Phenomena **86**, 107 (1997).
[29]A. J. Berry, H. S. C. O'Neill, K. D. Jayasuriya, S. J. Campbell, and G. J. Foran, Am. Mineral. **88**, 967 (2003).
[30]F. Galdenzi, G. Della Ventura, G. Cibin, S. Macis, and A. Marcelli, Radiat. Phys. Chem. **175**, 108088 (2020).
[31]B. Ravel and M. Newville, J. Synchrotron Radiat. **12**, 537 (2005).
[32]M. Blume, S. Geschwind, and Y. Yafet, Phys. Rev. **181**, 478 (1969).